Bridge Maintenance, Safety, Management, Life-Cycle Performance and Cost

Editors
Paulo J.S. Cruz, Dan M. Frangopol & Luis C. Neves

IABMAS
International Association for
Bridge Maintenance and Safety

Verifying design plans and detecting deficiencies in concrete bridge using GPR

L. Topczewski, F.M. Fernandes, P.J.S. Cruz & P.B. Lourenço
University of Minho, Department of Civil Engineering, Guimarães, Portugal

ABSTRACT: During the construction of concrete structures such as bridges, many deficiencies may occur due to an incorrect application or changes in the original design plans and construction errors. Frequently, areas with very poorly vibrated concrete, insufficiently grouted tendon ducts and incorrectly positioned reinforcement bars appear. Thus, the detection of these construction deficiencies is essential to prevent further damage to the bridge. Subsequently, a concrete specimen was prepared aimed at simulating some of the problems that can occur during the construction. The specimen was then mapped using a GPR system to check the effectiveness of this tool to provide information about those deficiencies. The acquisition was carried out in reflection mode and the results were further processed using 3D reconstruction software in order to obtain a more realistic and comprehensible image. These measurements showed rather good results. The 3D image provided much more detailed information about the elements placed inside the specimen relatively to 2D radargrams, which are generally used for primary target identification.

1 INTRODUCTION

An increasing number of researchers are using Ground Penetrating Radar (GPR) systems as a diagnostic and quality assurance of concrete structures (Maierhofer & Kind 2002, Giannopolous et al. 2002, Forde 2004). The use of this tool has been validated by numerous authors for the assessment of the metallic reinforcement bars (Maierhofer & Kind 2002, Maierhofer et al. 2003, Hugenschmidt 2002, Dérobert, 2002), in the inspection of grouting quality inside plastic tendon ducts (Giannopolous et al. 2002, Forde 2004), and in the diagnosis of damage in concrete structures (Maierhofer et al. 2003, Taffe et al. 2003). The inspection of bridge decks, particularly in the case of pre-stressed concrete bridges, is a critical task, but has been successfully carried out by many researchers (Scott et al. 2003, Hugenschmidt 2002) using GPR sounding with 3D image processing. Further details about this technique can be found in Kohl et al. (2003) and Valle et al. (2000).

The Portuguese Highway Administration has been looking for a fast and accurate way of obtaining information about the structural state of concrete bridges. This draw the attention of University of Minho, which decided to use GPR to verify its effectiveness in identifying the different materials, metallic reinforcement bars, plastic tendon ducts and other anomalies that can occur in such large and complex structures. Thus, a concrete specimen was built in laboratory environment and a number of typical elements were placed inside. GPR was then used to map all these features.

2 DESCRIPTION OF THE SPECIMEN AND METHODOLOGY

The concrete specimen that has been specially designed and built for this testing campaign in April 2004 aims to simulate a small part of a typical concrete bridge deck. It is a square with dimensions of 250 × 250 cm and a thickness of 32 cm. The elements that were placed inside were chosen among typical elements used in the construction of structural elements in reinforced and pre-stressed concrete bridge decks. A number of typical defects and anomalies that may occur deriving from errors during the construction were put in the specimen as well. A general view of the features inside the slab before being filled with concrete is illustrated in Figure 1a, while a general view of the final specimen is illustrated in Figure 1b.

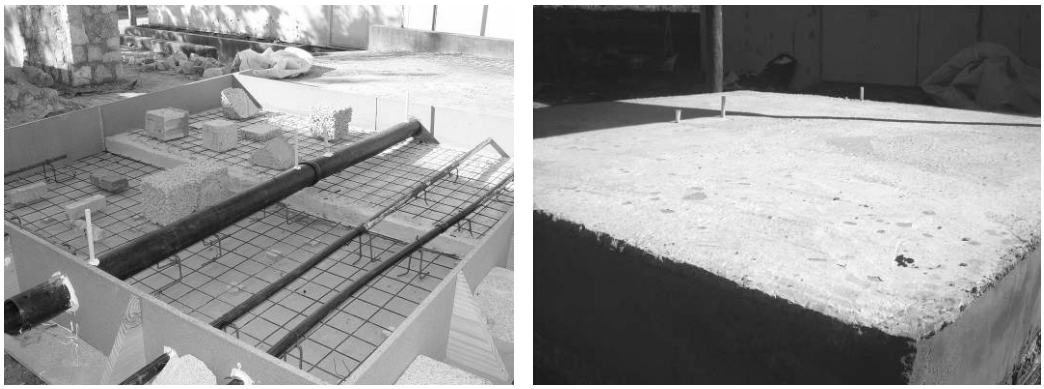

(a) (b)

Figure 1. General view of the concrete specimen. (a) Overview of the features and objects placed inside the specimen and (b) final view of the slab.

Inside the slab were placed three tendon ducts, in PVC, with 110 and 35 mm of diameter. The larger tendon duct is generally used for the introduction of post-tensioning cables, while the two smaller tendon ducts are simulating simple mono-cables, one in straight line and the other with curved path. The objective is to detect all tubes by radar and to verify if all tubes are correctly detected, with special attention to the curved tube. The measurements will be performed without cables inside the smaller tubes. However, in the largest one, half the tube is fully grouted with cement grout and the other half only half grouted in order to check the difference between fully filled and partially filled sections in tendon ducts. Several other deficiencies were simulated as well, such as the event of a poorly vibrated or lower density concrete, which was simulated by: blocks of concrete with insufficient binder (poor concrete), different density concrete (light-weight concrete), large voids, and blocks with inclined surfaces. Furhtermore, one empty bottle, one clay brick, wood and mortar prisms and two metallic bars were also putted in this specimen.

Aditionaly, a pre-casted concrete element was placed at the bottom of the specimen (Figure 1a) and occupies half of the total area of the slab. The thickness of this element is 7 cm, and the location inside the concrete specimen is illustrated in Figure 2.

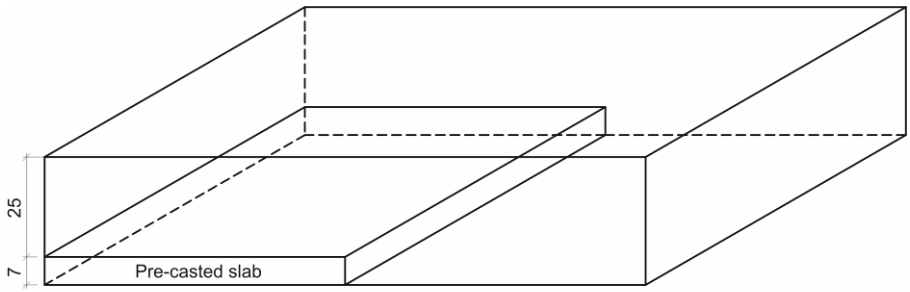

Figure 2. Location of the pre-casted element inside the concrete specimen.

The rest of the specimen is filled with pre-fabricated concrete. The concrete's class is C30/35 and was also used in the pre-casted element. No metallic reinforcement bars were used to build this specimen, only metallic grids were used in the bottom of the specimen and in the upper surface of the pre-casted slab in order to prevent premature cracking and increase the specimen's strength. The grid is constituted by metallic wires with 2 mm of diameter and squared cells with 15 cm of edge. An additional metallic piece was also provided in contact with the pre-casted element in order to be able to detect it more easily in the radargrams.

Concerning the GPR system used for the acquisition, the authors used the RAMAC/GPR from MALA Geoscience. The system was equipped with an antenna with a central frequency of 1.6 GHz, which was preferred due to the high resolution it provided and due to the small dimensions of the targets of this investigation. A digital hip-chain was used as positionning system and as pulse trigger.

Moreover, in order to construct good 3D images, a specific methodology was carried out. Thus, longitudinal 2D profiles closely spaced (5 cm apart) were acquired along the areas of interest. Such a density of longitudinal profiles was essential in order to obtain a realistic 3D image and necessary to map all possible elements. In Figure 3a is illustrated the grid drawn over the surface of the slab. Two areas of interest have been selected and are reported in Figure 3b: one is constituted by half the specimen (Area 1 in Figure 3b), where are located most of the deficiencies (poorly vibrated concrete, voids, etc.) and half of the pre-casted slab, and a second one (Area 2 in Figure 3b) that considers all the area of the specimen, specially the three tendon ducts. Radar acquisition in the area 2 was carried out in the direction perpendicular to the tendon ducts in order to maximize the return of the signal reflected by the tendon ducts. Area 1 was acquired parallely to the tendon ducts, so, the mapping of these elements was not considered.

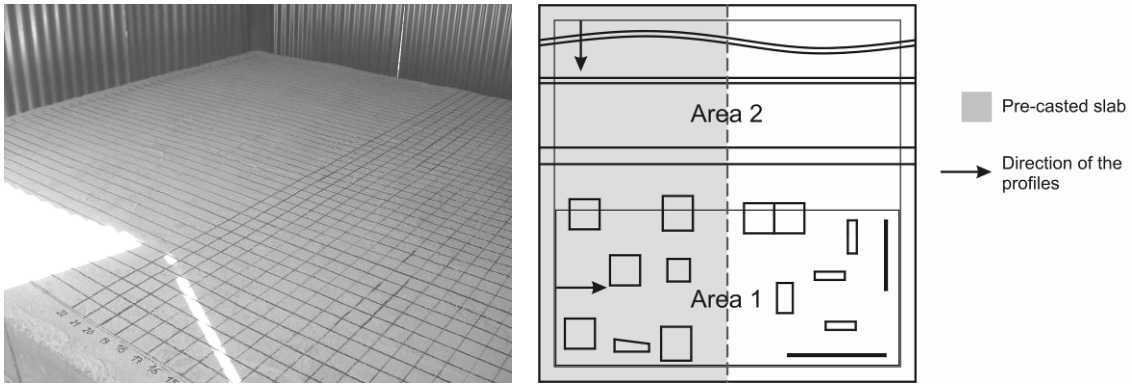

(a) (b)

Figure 3. 3D measurements. (a) Partial view of the grid drawn over the surface of the slab and (b) location of the areas of interest.

3 RESULTS

The analysis of the 2D profiles provided depth and location information about the elements located under each profile. Then, all profiles were joined in a 3D image, from where it was possible to extract slices at different depths. This provided additional information, such as shape and localization of the elements. The first area to be discussed will be area 1 followed by area 2, where the results from 3D reconstruction present indeed a clear advantage over 2D profiles in the specific case of bridge deck investigation.

3.1 *Results from Area 1*

The objective in this area was to determine the position and shape of all the elements (poorly vibrated concrete and voided prisms in particular) position of the opposite surface and the pre-casted slab. In Figure 4 is illustrated one radargram that shows the opposite surface at 7 ns of

depth. The opposite side was detected by means of the hyperbolas reflected by the metallic mesh, which was used to prevent concrete shrinkage, located at the bottom of the slab, almost in direct contact with the surface. As these hyperbolas were considered to correspond to the bottom of the slab, the 7 ns were considered to correspond to the 32 cm of thickness of the slab. This resulted in an average radiowave velocity of 9.2 cm/ns, which is rather low for concrete. Typical velocities in dry concrete are 9-13cm/ns. The pre-casted slab was detected in the first half of the radargram, at 5 ns from the surface, and a thickness around 1.5-2 ns (6.8-9.1 cm).

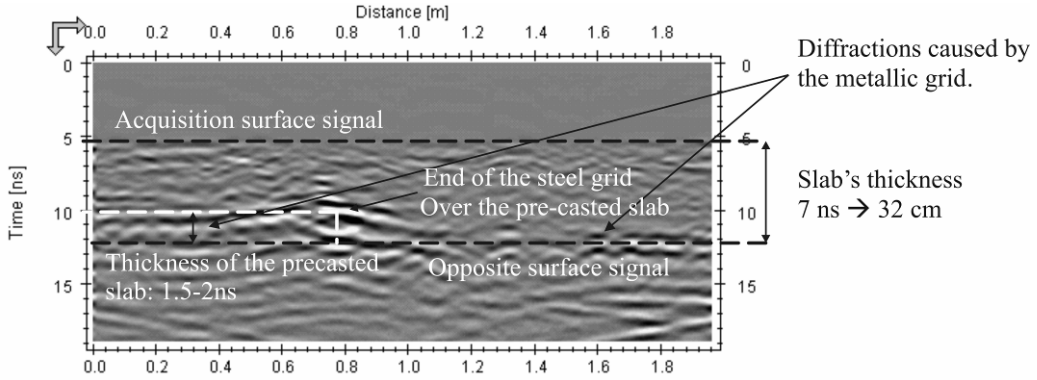

Figure 4. Detection of the opposite surface of the slab as well as the pre-casted slab.

In Figure 5 are shown additional profiles from where it is clear that poorly vibrated concrete and voided elements were successfully detected, as well as the metallic bar. From the radargrams below, the length of the concrete elements were acquired with rather satisfactory accuracy (the dashed boxes correspond to the dimensions of those elements). The height computed with the velocity of 9.2 cm/ns resulted in lower values than the real ones, which seem to suggest that the velocity within these concrete elements is slightly higher than in the rest of the whole specimen (radiowaves in porous concrete have a higher velocity of propagation). The position of objects is also rather accurate according to the location of two concrete blocks in the 22nd profile, relatively to the center axis. The radargram reported 12.5 cm while it was located at 12 cm (relatively to design plans). However, one element in each of the profiles from lines 4 and 22 was not detected. It must be noted that these elements have a triangular shape (see Figure 1a) and that the incident waves in such surfaces are scattered in a direction far from the receiver position. Thus, they are very difficult to detect.

Subsequently, the 3D image was build by performing linear interpolations between successive and closely spaced 2D radargrams. This way, it was possible to obtain a more realistic view of the data and, eventually, to better define the shapes and relative position of the objects previously detected with 2D profiles. The whole data is migrated in order to transform the diffraction hyperbolas in patterns closer to the shape of the objects they represent, and slices at different depths can be extracted to compare with the original design drawings. In Figure 6 two examples of time slices extracted from the main 3D volume are illustrated. Generally, a good correlation between the dimensions and relative position of single objects with the original design plans was obtained. However, in some cases, their relative position can differ quite substantially due to deviations caused by the filling of the formwork with concrete and due to the vibration process. On the top radargram of Figure 6 is illustrated a particular case where the original positions, in white, are different from the actual position, in black, detected by the antenna. However, not all elements were detected. Relatively to the shape of the objects, it depends exclusively in the effects caused by the migration algorithm, which concentrates energy in the apex of the events. Additionally, the length and the starting point of the profiles were not rigorously the same due to the positioning system used during the acquisition.

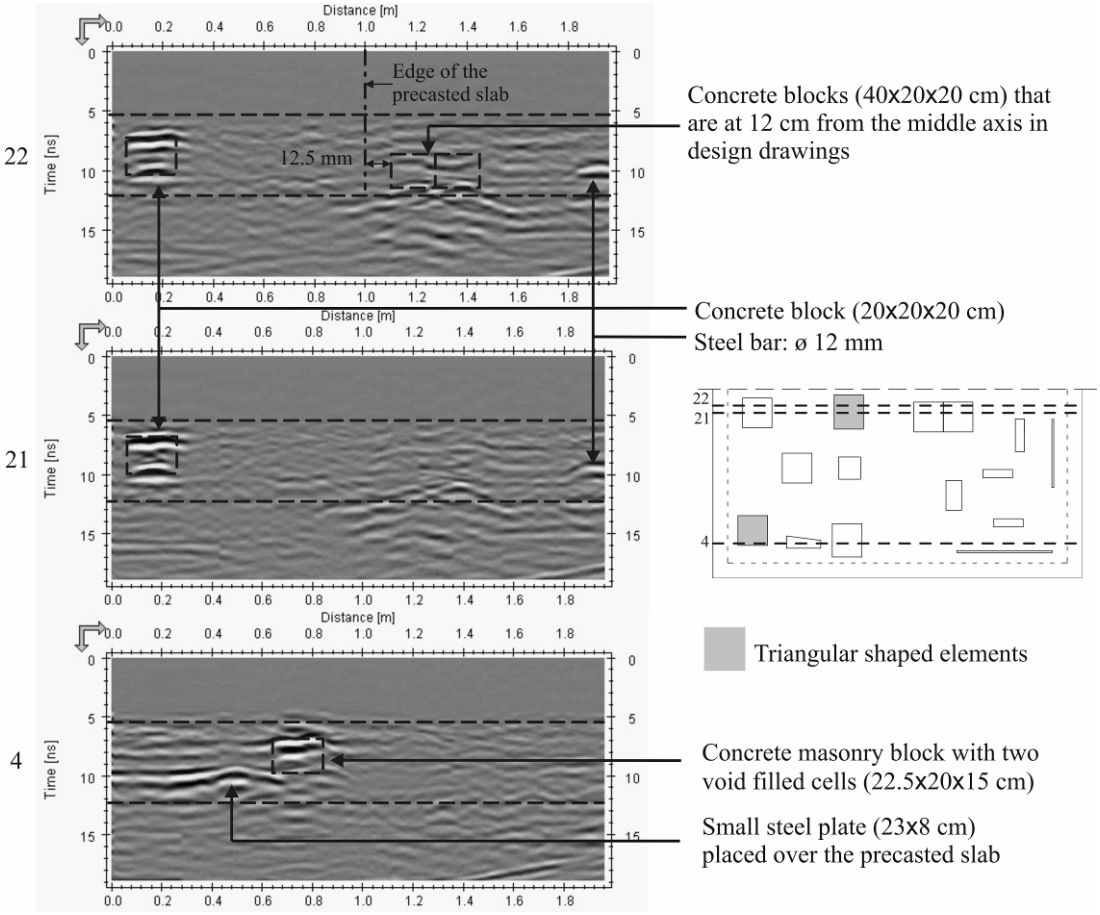

Figure 5. 2D profiles of the 22nd, 21st and 4th acquisition lines, respectivelly, from top to bottom.

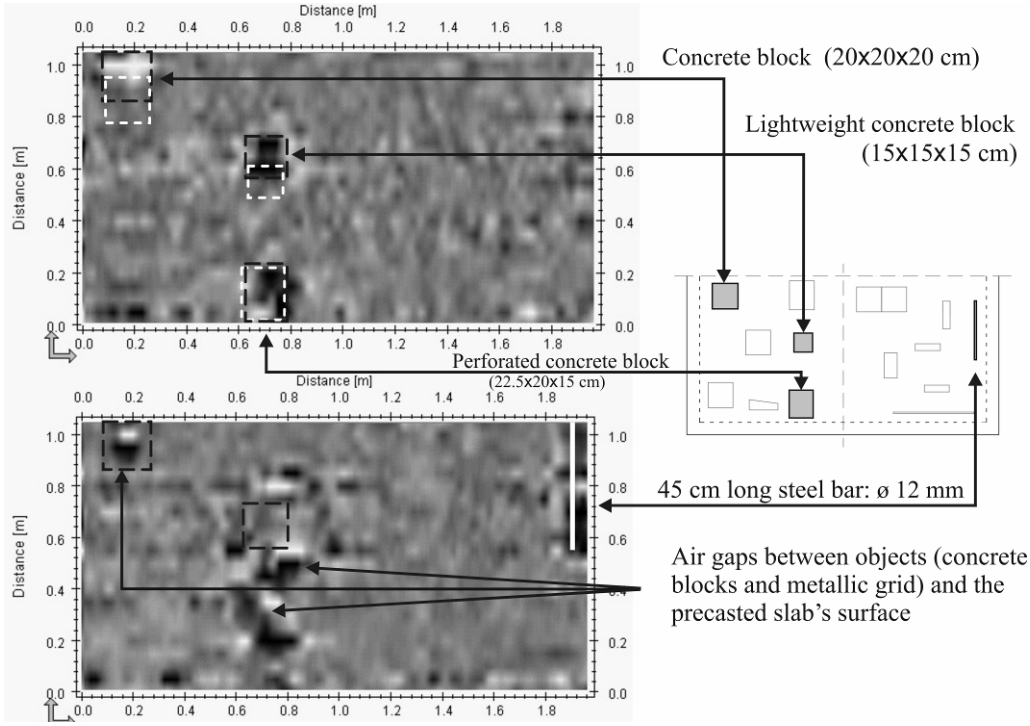

Figure 6. Interpolated time slices from the migrated 3D volume with accuratly positionned objects that are not in their original location. Depth of the slices: 10 and 18.5 cm, respectivelly, from top to bottom.

3.2 *Results from Area 2*

The second area considered for the investigation corresponds to the totality of the slab's surface (see Figure 3), with the objective of mapping the features located in the interior of the slab. In this case, particular interest lied on the detection of the three tendon ducts, especially in the correct acquisition of the curved shaped tendon duct and in the larger one, which has half and fully grouted sections. Such approach was already reported in Groenenboom et al. 2001.

The analysis of the normal 2D profiles showed that the three tendon ducts were detected in all cases. The radargram in Figure 7 illustrates the three tendon ducts, where it appears that the two smaller diameter tendon ducts (35 mm) are detected by their superior interface while, in the case of the larger diameter tendon duct (110 mm), both interfaces seemed to be detected. This phenomenon is associated to the short wavelength of the 1.6 GHz antenna, which is 18.75 cm, from where it results in an expectable resolution of 47 mm, taken as $\lambda/4$ (Forde 2004). Because the diameter of the smaller tendon ducts is inferior to 47 mm, the signal from the upper interface of the smaller tendon ducts would cover the lower interface signal, which happens effectively. Only the signals that were reflected by the boundaries of the largest tendon duct are both visible due to the fact that the distance between them is longer than the signal's expected resolution. However, this depends on the contrast between the tendon duct and the infill material (air, grout, or steel bar).

The analysis of the time slices gives good results as it was possible to resolve all intended targets, namely the three tendon ducts, and the position and shape of some of the other targets (not all targets were indeed resolved). In the following radargrams illustrated in Figure 8 are visible several concrete blocks as well as one of the reinforcement steel bars, the one that was perpendicular to the direction of radar acquisitions. The quadratic/rectangular shape of the objects is quite reasonably detected after the migration of the data. However, some of the objects placed in the interior of the concrete specimen were not exhibited. Most probably, some of them were not detected because they were oriented in parallel to the radar profiles (plastic bottle and clay brick), and others were two small or too deep to be reached by the radiowave (lightweight concrete cube, mortar and wood prisms) as well as lack of contrast (concrete cube with 5 cm of edge).

Moreover, the mapping of the three tendon ducts is shown in Figure 9, where it can be observed that all tendon ducts are correctly detected and the curvature of the curved tendon duct is well defined. Regarding the largest tendon duct, although it has been correctly detected, the intensity of the signal amplitude is not uniform along its entire length. As it can be seen in the 2nd and 3rd radargrams of Figure 9, the radiowave's energy seems to be higher in the bottom part of the section where the tendon duct's section is half grouted or half air filled. The air in that area could explain the higher energy due to the high contrast between dielectric constant of concrete ($\varepsilon_{r,\,concrete} = 6$) and air ($\varepsilon_{r,\,air} = 1$), which does not exist between concrete and grout. Thus, it seems possible to detect differently filled tendon ducts sections by analyzing the amplitudes of the reflected signals, although it has shown to be irregular as it can be seen in the first radargram of Figure 9.

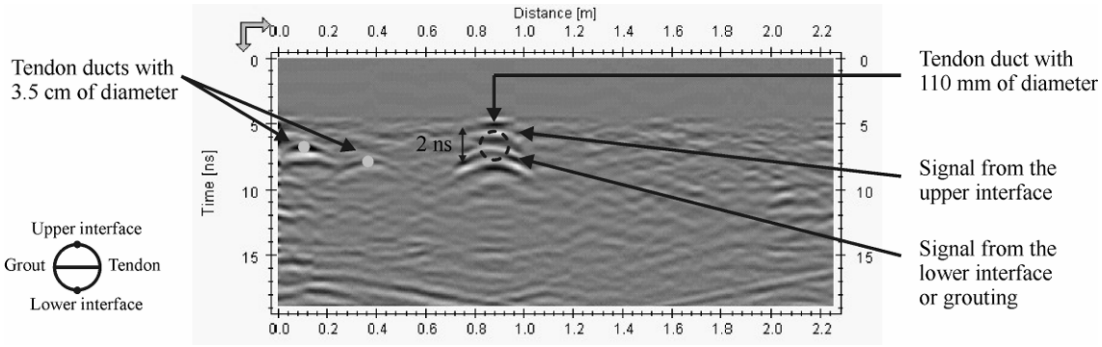

Figure 7. First profile at 10 cm from the border.

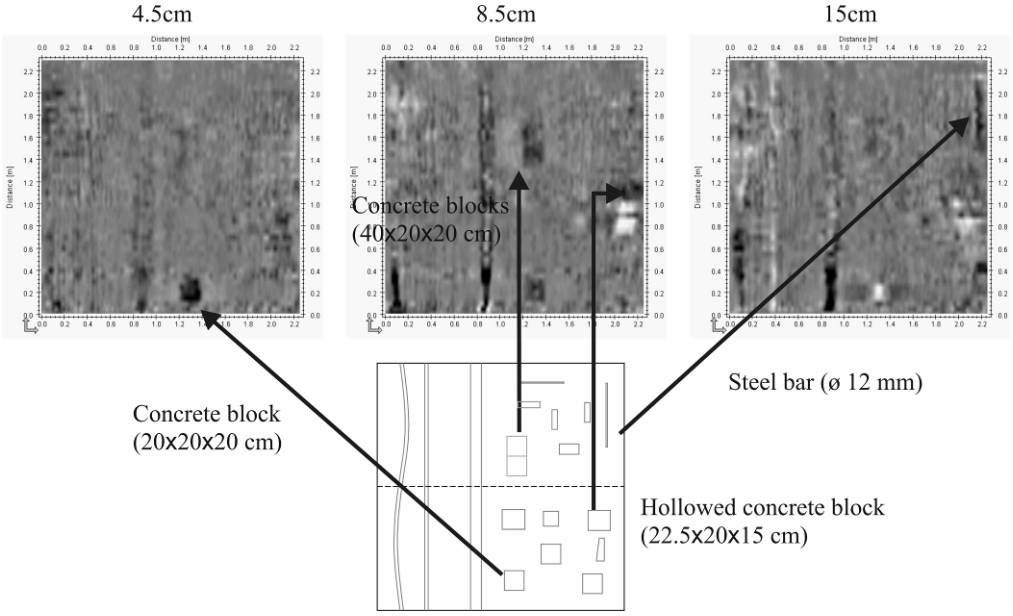

Figure 8. Time slices after migration where are observed some of the concrete blocks and the steel bar perpendicular to the acquisition direction.

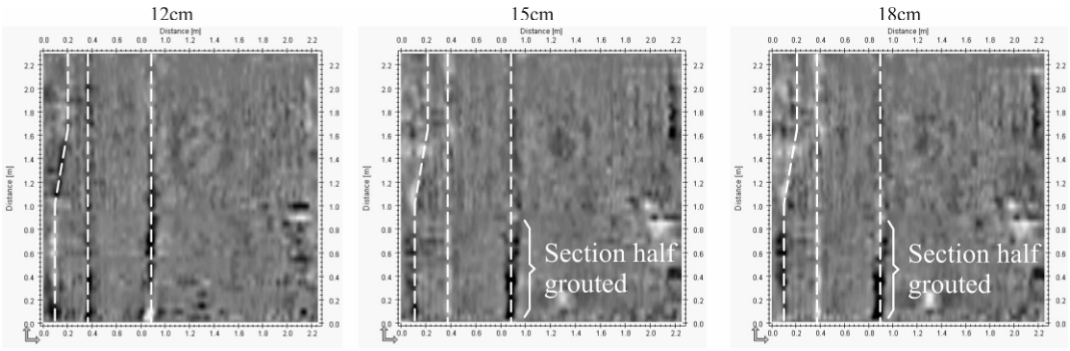

Figure 9. Radargrams showing the three tendon ducts.

4 CONCLUSIONS

The analysis of design conformity and mapping of deficiencies in concrete bridges is a matter of extreme importance for future maintenance. The use of GPR with 3D reconstruction showed good potential in the detection of the main structural elements as well as with the mapping of typical deficiencies. The antenna with a central frequency of 1.6 GHz exhibited very good resolution and high accuracy. The tendon ducts were all detected and the curvature of the curved tendon duct was correctly assessed.

However, not all targets were resolved, but the analysis pointed out several reasons to explain these results. Effectively, some of the targets were not detected due to its unfavorable orientation relatively to the direction of the profiling, which was the case of all objects parallel to the profiles. Because the profiles started and ended 10-15 cm after and before the specimen's border, some objects located very close to the edges of the specimen were not detected as well. Particularly the steel bar perpendicular to the tendon ducts. Moreover, the poor contrast between materials resulted in poor reflectivity and thus weak detection, particularly in the case of the lightweight concrete specimen. Additionally, the triangular shapes did not reflect favorably for detection by the radar signals, which resulted in the non detection of those objects.

5 ACKNOWLEDGMENTS

First author would like to acknowledge the support from "Sustainable Bridges" European project by the grant number FP6-PLT-01653. Second author would like to acknowledge the partial support from FCT (Portuguese Foundation for the Science and Technology) by the grant number POCTI SFRH/BD/6409/2001.

REFERENCES

Derobert, X. 2002. Comparison of NDT techniques on a post-tensioned beam before its autopsy. *NDT&E International* 35: 541-548.

Forde, M.C. 2004. Ground penetrating radar. Lecture Notes. TRB Annual Meeting. NDE Validation Center, USA.

Giannopolous A. et al 2002. GPR detection of voids in post-tensioned concrete bridge beams. *Proc. SPIE* 4758: 376-381

Groenenboom, J. et al. 2001. 3D GPR data acquisition and the influence of positioning errors on image quality, *Proc. EAGE* 63rd Conference and Technical Exhibition, 11-15 June, Amsterdam, 4 pp.

Hugenschmidt, J. 2002. Concrete bridge inspection with a mobile GPR system. *Construction and Building Materials* 16: 147-154.

Kohl, Ch. et al. 2003. 3D-visualisation of NDT data using a data fusion technique. *Insight* 45 (12): 800-808.

Maierhofer, Ch. & Kind, Th. 2002. Application of impulse radar for non-destructive investigation of concrete structures, *Proc. SPIE* 4758: 382-387.

Maierhofer, Ch. et al. 2003. Detection of shallow voids in concrete structures with impulse thermography and radar. *NDT&E International* 36: 257-263.

Reynolds, J. 1997. *An introduction to applied and environmental geophysics*. Chichester: John Wiley & Sons Ltd.

Scott, M. et al. 2003. A comparison of nondestructive evaluation methods for bridge deck assessment, *NDT&E International* 36: 245-255.

Taffe, A. et al. 2003. A Specimen for the improvement of NDT methods, Design and construction of a large concrete slab for NDT methods at BAM. *Proc. NDT-CE*, 16-19 September, Berlin, Germany.

Valle, S. et al. 2000. 2D and 3D focusing of ground penetrating radar data for NDT, *Proc. SPIE* 4084: 157-162.